Inorganic Chemistry

ARTICLE

pubs.acs.org/IC

Rationalization of the Lanthanide-Ion-Driven Magnetic Properties in a Series of 4f−5d Cyano-Bridged Chains

Stefania Tanase,*[,†] Marilena Ferbinteanu,*[,‡] and Fanica Cimpoesu[§]

[†]Van't Hoff Institute of Molecular Sciences, University of Amsterdam, Science Park 904, 1098 XH Amsterdam, The Netherlands

[‡]Faculty of Chemistry, Inorganic Chemistry Department, University of Bucharest, Dumbrava Rosie 23, Bucharest 020462, Romania

[§]Institute of Physical Chemistry, Splaiul Independentei 202, Bucharest 060021, Romania

Supporting Information

ABSTRACT: Magnetic properties of new d−f cyanido-bridged 1D assemblies $[RE(pzam)_3(H_2O)W(CN)_8]\cdot H_2O$ (RE(III) = Gd, **1**, Tb, **2**, Dy, **3**; pzam = pyrazine-2-carboxamide) were studied by temperature- and field-dependent magnetization measurements. No evidence for 3D interchain magnetic ordering is found above 2 K. Multiconfiguration ab initio calculations and subsequent modeling afforded simulation of the weak zero-field splitting effect in **1** and discussion of magnetic anisotropy in the f units of compounds **2** and **3**. A semiquantitative corroboration with the experimental magnetic measurements is presented, performing the simulation of magnetic susceptibility vs temperature and magnetization vs field variation. The association into molecular and supramolecular architectures is analyzed by means of energy decomposition subsequent to the DFT calculations on idealized molecular models extracted from the experimental chain structure.

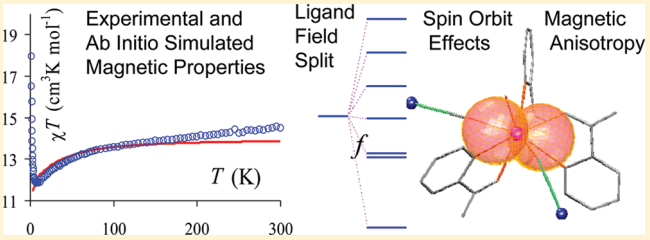

1. INTRODUCTION

Compounds containing lanthanide ions are widely studied because of the intrinsic magnetic anisotropy of the lanthanide ion.[1,2] This is a key factor for designing the so-called single-molecule magnets (SMM),[3,4] materials with promising applications in microtechnologies. The challenge brought by lanthanides inside the SMM topic is that the phenomenon appears in a large range of complexes, both at high nuclearities[5] and also at the minimal level of binuclears[6] or even in mononuclear compounds.[7] Among the various possible molecular architectures, the one-dimensional (1D) polymers represent a special case because of their fairly simple topology. On one hand, the chain structure allows a relatively simple scheme of parametrization, with one or two exchange coupling constants. On the other hand, it raises the problem of dealing with infinite systems when tackling their modeling. In addition, the lanthanide ions bring a challenge also from the perspective of supramolecular and crystal engineering concepts. This is due to the preponderantly ionic regime of their bonding that yields a rather extreme versatility in the constitution and conformation of the coordination spheres. The result is a low predictability of the magnetic interactions especially when considering the role of environment proximities, such as solvents, hydrogen bonds, or other coordination units.[8]

Using ab initio calculation and appropriate interpretations to meet the chemical intuition and physical meaning, we bring here case studies rationalizing the magnetism and association effects in f units and d−f assemblies. The ab initio electron structure methods have become increasingly popular and frequently used nowadays. This is likewise an acknowledged complement of the modern experimental chemistry.[9] However, many problems of the magnetism are beyond the current routine of available computer packages. Particularly, the lanthanide(III) compounds are difficult to treat with routine ab initio methods. This is due to hidden technical difficulties residing in the non-aufbau configuration of lanthanide(III) compounds that induces numerical instabilities in regular iterative procedures. The situation is in sharp contrast with awareness about the utility of ab initio methods themselves as well as with the growing importance of lanthanides in the field of molecular magnetism. Previously, we reported original conceptual and methodological developments[10] applying the state of the art approach of ab initio calculations to f and d−f complexes. The procedures were used to explain the ferromagnetism in prototypical Cu(II)−Gd(III) complexes,[10] the SMM behavior of a new Fe(III)−Dy(III) dimer,[11] as well as treatments related to the magnetic anisotropy of lanthanide ions in given coordination spheres.[12,13] Here, we extend our studies to a new class of d−f systems, namely, 1D assemblies.

The first 1D compounds containing lanthanide(III) ions and transition metal ions were reported by Kahn et al.[14] These compounds have a ladder-like structure composed of alternating lanthanide(III) ions and $[Cu(opba)]^{2-}$ units. These systems undergo long-range magnetic order at temperatures below 2 K. Hexacyanidometallates, $[M(CN)_6]^{3-}$ (M(III) = Fe, Mn, Cr, Co), have also shown their ability to act as efficient bridging units

Received: July 6, 2011
Published: August 26, 2011

toward lanthanide(III) ions and to form 1D compounds.[15] Many other 1D systems emerged in the lanthanide chemistry of the past decade, bringing diverse knowledge on the related magnetism and assembling factors.[16] Nevertheless, analysis of the magnetic properties has proven to be difficult due to the weak magnetic interactions and not detailed enough to define correctly the magnetic dimensionality of the systems. Therefore, the classical ligand field theory[17,18] might be of great help in rationalizing the energies of the low-lying levels of both the transition metal and the lanthanide ions.[19] The magnetism of lanthanide ions is in the vast majority of reports characterized qualitatively and descriptively. However, several interesting approaches attempted a ligand field-based fit of magnetic properties.[20,21] In the case of Ishikawa's phthalocyaninato systems,[20] the approach benefits from the advent of high symmetry, the parametrization having therefore a reduced number of parameters. However, in the case of low-symmetry complexes,[21] the modeling implies many parameters and the question of assessing the general reliability or whether a certain fit is unique may remain open to further debate and methodological explorations.

Previously, we reported a detailed experimental study of the magnetic properties of one-dimensional d−f cyanido-bridged assemblies derived from $[M(CN)_8]^{3-}$ and $[RE(pzam)_3]^{3+}$ building blocks (M = Mo(V), W(V), RE = rare earth ions, pzam = pyrazine-2-carboxamide).[22,23] In several cases, we performed the fit of the exchange interactions between neighboring metal ions and their correlation to the structure. In this paper, we report experimental and theoretical studies on the isostructural family $[RE(pzam)_3(H_2O)W(CN)_8]\cdot H_2O$ (RE(III) = Gd, Tb, Dy). In addition, we discuss the magnetic data in terms of the intrinsic anisotropy of the lanthanide ions as determined by the ligand field.

2. EXPERIMENTAL AND MODELING DETAILS

2.1. Synthesis and Characterization. Compounds $[RE(pzam)_3(H_2O)W(CN)_8]\cdot H_2O$ (RE(III) = Gd, **1**, Tb, **2**, Dy, **3**) were prepared using an earlier reported procedure.[22,23] Elemental analysis, IR spectroscopy, and X-ray powder diffraction studies indicated that they are isostructural with the family $[RE(pzam)_3(H_2O)Mo(CN)_8]\cdot H_2O$. They crystallize in the space group *Pna*21, and their crystal structure is formed by chains of cyanido-bridged alternating arrays of $[W(CN)_8]^{3-}$ and $[RE(pzam)_3(H_2O)]^{3+}$ fragments running along the *b* crystallographic axis.[22,23] Each chain is surrounded by six other equivalent chains through hydrogen-bonding interactions, giving rise to a three-dimensional network.

2.2. Physical Methods. Temperature-dependent magnetic susceptibility and magnetization measurements were performed with a Quantum Design MPMS-5 5T SQUID magnetometer. The susceptibility is recorded at the 0.1 T field in the temperature range 1.8−300 K, the magnetization measurements being taken at 2 and 4 K in the range 0−5 T. Samples were embedded in solid icosane to prevent torquing. Data were corrected for the magnetization of the sample holder and for diamagnetic contributions as estimated from the Pascal constants.

2.3. Ab Initio Calculations. The calculations were performed on correspondingly cut and customized molecular fragments. The systems were taken at the experimental geometry of complexes, replacing the corresponding W−CN from the chain by terminating Li−CN groups. The use of Li as surrogate has the advantage of mimicking the polarization effects of the bridge in a better way than a simple CN^- anionic cut of the structure. Thus, $[RE(pzam)_3(H_2O)(NCLi)_2]^{3+}$ fragments were used to investigate the mononuclear lanthanide units (replacing both W−CN contacts with Li−CN prosthetics) and $[RE(pzam)_3(H_2O)(NCLi)][W(CN)_8]$ as models for dimeric sequences (replacing with Li−CN only one W−CN bridge).

To discuss the magnetic anisotropy of lanthanide units we carried out CASSCF (complete active space self-consistent field) calculations as well as ab initio spin−orbit (SO) treatments. The calculations were performed with the GAMESS program.[24] We used SBKJC[25] effective core potentials and basis sets for lanthanides (Gd, Tb, Dy) and W and 6-31G* basis set for the ligands. The CASSCF calculations are driven in a nonstandard manner due to specifics of the electronic structure of the lanthanide ions. The main clue consists of avoiding the customary single-determinant stage that usually precedes CASSCF calculations as a preliminary step in defining and choosing the active set. In turn, we prepare an orbital set resulted from merging the fragments: the separate f centers, the ligands, and the d complexes, if the case. The procedure is performed with the help of a separate code, developed by ourselves, which reads the output eigenvectors of components and writes the cumulated vector, to serve as further input. In this way, a zero-order LCAO matrix of the whole complex is built with initial zero block matrices between fragments serving as the start of multiconfiguration procedures. This methodology (applied in sections 3.1 and 3.2) is in line with the physical truth that lanthanide ions are in fact weakly interacting systems. The CASSCF-SO ab initio calculations performed for the free ion reproduce well the experimental atomic terms of the lanthanide ions, assessing the reliability of the chosen setting. However, this assessment failed for the case W(V) ion, probably due to problems in the SBKJC basis set and pseudopotentials of the tungsten. In these circumstances we aimed the calculations to the effects of ligand field and anisotropy inside the lanthanide units, confining ourselves not to compute the Tb(III)−W(V) dimer models.

We also studied (section 3.3) the association energy of ligand to the metal ions and mutual assembling of d and f complex units. Since the f shell does not contribute to the bonding we used a simpler route, employing Lu(III) as surrogate for the lanthanide site in density functional theory (DFT) calculations. Lu(III) has the advantage of having the f shell fully occupied, avoiding in this way complications related to the non-aufbau nature of the f compounds. In turn, the bonding effects due to the valence shell are semiquantitatively well accounted with Lu(III) as representative of the other lanthanides.[13] The DFT calculations in the model Lu(III) complexes were done with the ADF (Amsterdam Density Functional) code[26] using the gradient-corrected Becke−Perdew[27] functional and TZP basis sets.

2.4. Ab Initio Simulation of Magnetic Properties. A special methodological advance is the ab initio simulation of the magnetization and susceptibility. The algorithm is a nonstandard implementation, based on the extraction of corresponding data from the black box of CASSCF-SO calculations. The SO module permits obtaining the matrix elements from the L_x, L_y, and L_z operators and therefore construction of the orbital components of the Zeeman Hamiltonian. At the same time, obtaining the spin Zeeman components is straightforward. Adding the constructed orbital and spin-type Zeeman matrices to the computed CASSCF-SO matrix, one may introduce the magnetic field dependence in the full spectrum of states. For a given state, indexed by "*i*", the magnetization is computed as the derivative with respect to the magnetic field applied from a given direction, expressed by the θ,φ polar coordinates

$$\mu_i(\theta,\varphi) = -\left(\frac{dE_i}{dB}\right)_{\theta,\varphi} \quad (1)$$

The polar diagram of the module of $\mu_i(\theta,\varphi)$ dependence yields the magnetization surface of the given "*i*" state. The maximal extension of the lobes of the magnetization surfaces can be formally correlated with effective $g_J\cdot J_z$ amounts for the given spin−orbit component. For isotropic states, i.e., multiplets with good *J* or *S* quantum numbers, the magnetization of the components results as spheres with $g_J\cdot J_z$ or $g_S\cdot S_z$ radii. This implementation enables also the ab initio simulation of global

dx.doi.org/10.1021/ic201427w |*Inorg. Chem.* 2011, 50, 9678–9687

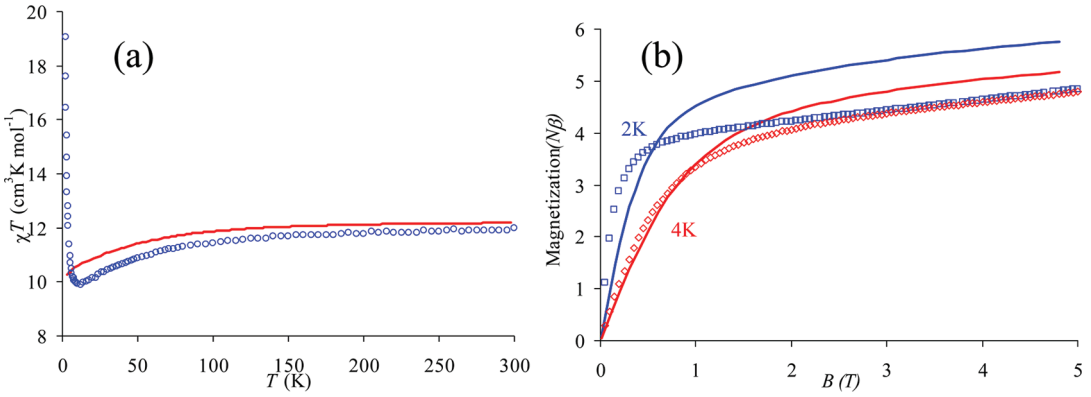

Figure 1. (a) Temperature dependence of χT for compound **2**: experimental (blue circles) and simulated (continuous red line). (b) Field dependence of the magnetization recorded at 2 (blue squares) and 4 K (red diamonds) and the simulated curves (blue and red lines). The modeled curves consist in the ab initio estimation of susceptibility and magnetization for the Tb(III) complex unit, summed with a $S = 1/2$ paramagnet for the W(V) component (i.e., a constant in χT line and Brillouin functions for magnetization). The simulated lines are not object of a fit, resulting from the first-principles approach. The accordance to experiment is semiquantitative, having a slight overestimation of all curve profiles while a good retrieval of the qualitative pattern.

magnetic properties, such as magnetization as a function of the field and susceptibility as a function of temperature. For this purpose, it is convenient to work with the state function sum, Z, defined with respect to the full ab initio spectrum

$$Z(\theta, \varphi, B) = \sum_i \exp\left(-\frac{E_i(\theta, \varphi, B)}{k_B T}\right) \quad (2)$$

The dependence of the E_i state energy with the magnetic field, expressed as modulus B and orientation (via the θ,φ polar coordinates), is implemented as explained previously. The magnetization and susceptibility are expressed as first and, respectively, second derivatives of the Z function, with respect of the magnetic field (see Supporting Information). Because these quantities are anisotropic, the simulation is completed integrating over the θ,φ coordinates. The numerical differentiation is realized with a $dB = 0.001$ T infinitesimal step. The numerical integration is made over a 24×48 mesh, with respect of the θ,φ angles.

3. RESULTS AND DISCUSSION

3.1. Temperature- and Field-Dependent Magnetization Studies. A brief description of the magnetic properties of compound **1** was reported previously.[23] The temperature dependence of the magnetization has been analyzed in terms of the semiclasical Seiden's model,[28] and it revealed the presence of weak antiferromagnetic interactions between Gd(III) and W(V) ($J_{GdW} = -0.76$ cm^{-1}). Here, we performed a reconsideration of the fit in the frame of the Heisenberg Hamiltonian amended with a zero-field splitting (ZFS) part. We obtained comparable results, $J_{GdW} = -0.54$ cm^{-1} and $D = 0.02$ cm^{-1}. Though small, the ZFS is in line with the results of ab initio estimation. We performed the modeling on the oligomeric sequence $(Gd-W)_3$ taking χT as the average of chain and cycle cases. Higher topologies are not easily approachable in the iterative fit procedures because of exponential growth in Hamiltonian matrix dimensions. We verified at the noniterative level that the $(Gd-W)_4$ and $(Gd-W)_3$ simulations are practically coincident. The revisiting of the data was important due to the possible limitations of the Seiden model, assuming the hypothesis of classical spin on Gd(III), while the 1/2 component of the chain is treated as a quantum object.

The magnetism of the other systems discussed here is more complicated due to the intrinsic anisotropy of lanthanide ions. The experimental magnetization and susceptibility data are corroborated with simulations resulting from ab initio methods, following the above-mentioned methodology. For compound **2**, the temperature dependence of χT is given in Figure 1a. The room-temperature χT value of 11.97 cm^3·K·mol^{-1} is close to the expected value of 12.19 cm^3·K·mol^{-1} taken as the sum of noninteracting ($J_{Tb} = 6$, $g_{Tb} = 3/2$) and W(V) ($S_W = 1/2$, $g_W = 2$). Here, we use the J notation for designing the momentum resulting from orbital and spin coupling. This value remains almost constant down to ca. 150 K, where it starts to decrease, reaching a minimum value of 10.16 cm^3·K·mol^{-1} at 12 K. Below this temperature, the χT product increases markedly and reaches a value of 23.66 cm^3·K·mol^{-1} at 1.8 K. This behavior resembles that observed for the analogous compound containing Mo(V) instead of W(V).[22a] The high χT sequence below 12 K can be attributed to the ferromagnetic or ferrimagnetic ordering between Tb(III) and W(V). Since the exchange coupling is presumably small, it is superseded at larger temperatures by thermal disorder, so that approximately above 10 K the curve can be treated as the sum of the Tb(III) and W(V) ions, the main pattern being determined by the anisotropy of the lanthanide ion. This fact is supported comparing the experimental magnetism with those simulated summing the ab initio estimation for the Tb(III) complex and W(V) as a simple paramagnet. In spite of a slight overestimation, the simulated curve parallels well the experimental one certifying, at one hand, the reliability of the computation approach and, on the other hand, the fact that the lanthanide ions drive the main part of the curve. The simulations do not reproduce the nonmonotonous behavior at low temperature, sustaining then the point that this part is due to the exchange effects. Note that the theoretical simulation does not imply any fit, being directly based on the amounts extracted from the black box of ab initio calculations.

The field dependence of the magnetization for **2** was measured at 2 and 4 K, as shown in Figure 1b. From the magnetization data measured at 2 K it appears that a field of 2 T is needed to saturate the total net magnetization of the Tb(III) and W(V) moments. The subsequent slow and nearly linear increase of magnetization up to 5 T arises from the contributions from the excited levels (see Figure 1b). The modeled curves, consisting of ab initio simulation for the Tb(III) ion summed with a simple Brillouin function, are also paralleling the experimental data, with a certain overestimation of the plateaus, as in the case of the χT curve.

dx.doi.org/10.1021/ic201427w |*Inorg. Chem.* 2011, 50, 9678–9687

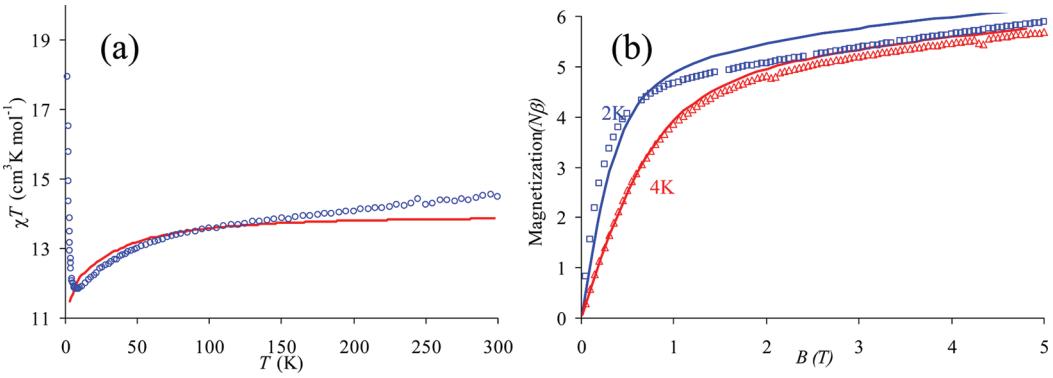

Figure 2. (a) Temperature dependence of $\chi_M T$ for compound **3**: experimental (blue circles) and simulated (continuous red line). (b) Field dependence of the magnetization recorded at 2 (blue squares) and 4 K (red triangles) and the simulated curves (blue and red lines).

The temperature-dependent magnetic susceptibility data for **3** are shown in Figure 2a as a χT vs T plot. At 300 K, the product χT is equal to 14.47 $cm^3 \cdot K \cdot mol^{-1}$, a value which is close to the 14.547 $cm^3 \cdot K \cdot mol^{-1}$ amount resulting as the sum of theoretical values of noninteracting ions, Dy(III) (with ideal quantum numbers J_{Dy} = 15/2, g_{Dy} = 4/3) and W(V) as 1/2 spin. By lowering the temperature, the product χT decreases progressively, reaching a value of 11.83 $cm^3 \cdot K \cdot mol^{-1}$ at ca. 8 K. Then it increases to about 17.94 $cm^3 \cdot K \cdot mol^{-1}$ at 1.8 K. The field dependence of the magnetization at low temperature is shown in Figure 2b. Following a procedure as described above for **2**, the experimental magnetic data are compared with simulations having as input the output of ab initio results of the lanthanide complex unit. The W(V) contribution is additively considered as a paramagnet. The sum of independent subsystems is a crude approximation, but it can be considered as reasonable at larger temperatures or magnetic fields, these external actions effectively decoupling the role of small exchange interactions. As in the previous case, the simulation based on the assumption of lanthanide leading magnetism is proved true above 10 K, while this does not account for the high χT values of the lower T zone. Therefore, we conclude this effect assignable to the exchange effects. Because of certain cautions in the reliability of ab initio account of the W(V) ion and $[W(CN)_8]^{3-}$ units, as mentioned in the above technical section, we will not approach here the exchange effects at the ab initio level.

3.2. Ab Initio Treatment of the Lanthanide Units. The above section illustrated the possibility of using the ab initio output for a realistic description of the magnetic properties. The good agreement between experimental and first-principles simulations can be assigned to the capacity of the electron structure methods to account well for all the effects competing inside the given f complexes. At a conceptual level, the ligand field (LF) and spin−orbit (SO) effects are the causal elements for the magnetic and optical properties of the mononuclear lanthanide units. For reasons related with the unavoidable complexity of the mathematical apparatus needed for the phenomenological account of the f shell,[17] the ligand field for lanthanides is less accessible than the more popular versions of LF models, devoted for d systems.[18] There are no simple intuitive rules to qualitatively guess the ligand field scheme of a given lanthanide complex. Besides, the theory demands, in general, many parameters.[17] The possibility to use the ab initio methods to skip the intrinsic complexities of the traditional LF models, having a reasonable account of related effects, directly from first principles, is an interesting and a convenient way. As mentioned previously, the ab initio approach of the lanthanide complexes is not straightforward, implying nonroutine preliminaries. However, this complexity is not insurmountable and must not be conceived as the incapacity of the existing methods to treat the f complexes, the CASSCF ones being perfectly suited for this purpose. As pointed out, it is merely a problem of appropriate preparation of the starting orbitals rather than a problem of the calculation itself. We encompassed this step devising fragment merged orbitals that place the pure f orbitals directly in the active space. At the end of the CASSCF iterations, the almost pure f orbitals are retrieved from the set of canonical orbitals.

We opine that the further increments of second-order perturbation theory type (PT2)[29] devised to introduce supplements of the so-called nondynamical correlation effects,[30] a posteriori to a multiconfiguration calculation, are not required for a reliable semiquantitative account of the LF and exchange effects in f and d−f complexes. In a previous paper, where the methodology for the ab initio approach of lanthanide complexes was devised,[10] we obtained comparable results at both the CASSCF and the CASPT2 levels. We do not exclude the possibility that in certain circumstances, or for other effects, the PT2 postiterative increments may be necessary. Nevertheless, in the basic respects of the LF for the f shell, such corrections are not vital. Even though the LF gaps on the f shell are relatively small, their main source is yet related with the interatomic integrals contained in the Hamiltonians of CASSCF methods, and this computational level is sufficient for insights oriented on the chemical meaning and retrieval of basic mechanisms. Besides, being nonvariational and tributary various conventions in introducing the perturbation increments, the PT2 methods may complicate the scheme in an unnecessary manner. We consider that once the problem of starting the iterations with well-defined active orbitals has been resolved, the lanthanide complexes can be treated with moderate computational effort by known multiconfigurational procedures and using rather standard basis sets, such as the effective core potential[20] ones.

On the basis of the discussion above, we performed calculations on the $[RE(pzam)_3(H_2O)(NCLi)_2]^{3+}$ fragments (RE = Gd, Tb, Dy) (see Experimental and Modeling Details section for details). The CASSCF(n,7) calculations (e.g., with n = 8 for Tb and 9 for Dy) correspond to the full configuration interaction related to the ground state terms of the f^n lanthanide configurations. Specifically, the optimized orbitals for the Tb(III) system were taken as state average over 7 states corresponding to the ^7F

dx.doi.org/10.1021/ic201427w |*Inorg. Chem.* 2011, 50, 9678–9687

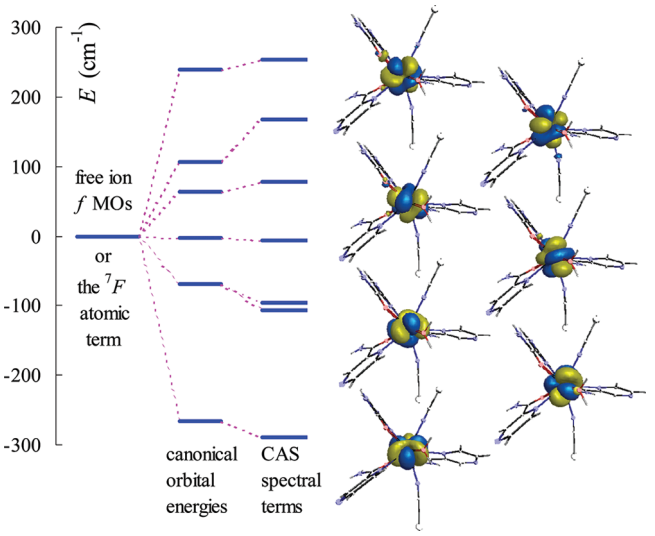

Figure 3. Ligand field rationalization of the results from CASSCF calculations on the Tb(III) unit of the system **2**. MO and spectral term energies are conventionally shifted with the barycenter at the zero point. The CAS spectral terms reflect directly the LF scheme as the split of the ^7F term of the free Tb(III) ion. The canonical MO energies can also be taken, in this case, as an approximation of the LF effects.

atomic term, while for Dy(III) they were obtained as an average over 11 orbital states, related to the free ion ^6H term. The CASSCF calculations in the actual environment retrieve well the ligand field (LF) regime, yielding a total gap of about 540 cm^{-1} for the ^7F multiplet of Tb(III) and 450 cm^{-1} for the ^6H term of the Dy(III), i.e., in accordance with the expected range.[20]

The Tb(III) unit of compound **2** is best suited to investigate the LF scheme in the considered series of isostructural complexes, the result being extrapolable for other congeners also. The f^8 configuration of the Tb(III) (i.e., a $7\alpha + 1\beta$ scheme) gives rise to a ^7F spectral term whose computed splitting expresses directly the LF effect on the f shell. The seven levels accounted for by the CASSCF calculation are based on configurations resulting from the successive placement of the β electron along the series of canonical MOs. Each ith level has as the main component (with mixing coefficients between 0.95 and 0.99) the configuration with the β electron in the ith canonical MO. In this circumstance, the spacing inside the computed CASSCF terms can be assigned to a LF scheme with one-electron effective nature. The energies of canonical MOs do not have direct physical meaning, being the subject of certain conventions, and as a matter of principle should not be used for LF purposes. However, in the actual case one may observe a good parallelism between the orbital-based schemes the more realistic one based on the computed spectral terms. The energy levels and contour of the orbitals are presented in Figure 3. The canonical MOs are almost pure f atomic orbitals. The molecular unit has no symmetry, and the orbitals are presented as a mixture of standard f shapes. Some of them show six lobes, while others with more deformed appearance can be described as a combination of eight lobe and six lobe elements. Considering that the cyanide ligands are exerting the strongest LF perturbation, one may see that the highest energy results for the orbitals having lobes directed toward the NC moieties while the lowest energy is assigned to an orbital with lobes escaping in between the donors. The canonical orbitals of the other systems show a pattern similar to the Tb(III) system, suggesting therefore a similar LF scheme throughout all the isostructural series.

We present in the following the theoretical approach to the magnetic anisotropy in the considered lanthanide compounds. For the Tb(III) system, the CASSCF-SO calculation over 49 states (i.e., the 7×7 total spin−orbital multiplicity of the ^7F term) yields a lower subset of 13 levels, mimicking the split of the $J = 6$ magnetic ground state. In this series, certain sequences are quite close to effective double degeneracy, i.e., 0.2 cm^{-1} between the 1st and 2nd levels or 1.2 cm^{-1} between the 12th and 13th ones, other couples being formed within the 10−20 cm^{-1} mutual gap. For the Dy(III) system, the CASSCF-SO calculations implied 66 states (i.e., the 6×11 count, corresponding to the ^6H ground term). The first 16 levels correspond to the splitting of the $J = 15/2$ formal spin−orbit state, as a consequence of the LF imposed over the spin−orbit coupling. The computed level energies are organized in 8 degenerate pairs, formally assignable to the $\pm J_z$ components. Nevertheless, such a relationship is merely allusive, because the J_z projections are not good quantum numbers. The anisotropy of the lowest levels of Tb(III) and Dy(III) is illustrated in Figure 4, drawing the corresponding magnetization surface with two lobe shapes. In the 3D frame represented in Bohr magneton units, the molecular skeleton is immersed in relative scaling. The magnetization surfaces can be understood as the response of the system in acquiring a magnetic moment when a probe field is applied from the respective direction. Thus, we apply a dB field from a given direction expressed by the θ,φ polar coordinates and obtain a $M = |dE/dB|$ response. We construct with this amount a polar diagram $M(\theta,\varphi)$, where the quantity M is the length from the center to the drawn surface, along the given direction. The direction of maximal elongation corresponds to the easy magnetization axis. On the contrary, a magnetic field applied in the nodal planes will get no magnetic response from the system. The orientation of the magnetization lobes represents valuable nontrivial results. This is determined in a complicated manner by the ligand field in the computed unit and the electron count of the f configuration.

If we attempt rationalizing the scheme in terms of the J_z quantum numbers, the maximal extension of magnetization lobes can be formally assigned to the $g_J J_z$ amounts. For the ground state couple of the Tb(III) complex, the magnetization surfaces show the largest lobes (in comparison to those of higher states), about 5.8 μB, meaning that we shall consider these as the ± 6 components. However, this magnitude is smaller than those obtained with the ideal $g_J = 3/2$ for Tb(III). The situation looks like having a Landé factor reduced to an almost orbital-like $g \approx 1$ value if formally the lowest couple to the ± 6 components or like a reduction of the effective projection itself. This fact as well the nonmonotonous distribution of the magnitude of the lobes along the spectrum of the $^7F_6$ term split in the complex, as seen in Figure 5, illustrates the intricacies of the combined effect of LF and SO actions.

For Dy(III), $g_J \approx 4/3-1.33$ and the maximal projection $\pm 15/2$ gives the 10 μ_B amount of magnetization. The actual maximal amplitude of the depicted lobes (8.5 μ_B) is formally assignable to a reduction at $g \approx 1.13$ of the Landé factor. The magnetization tensors are identical, in pairs, for the doubly degenerate states resulting from the CASSCF-SO approach of the Dy(III) complex. This is also closely similar for the near-degenerate couples revealed in the Tb(III) computation.

Figure 5 shows the spectrum of the 13 states discussed for the Tb(III) system (certain levels are superposed due to quasi-degeneracy). On the right side of the diagram, we present the magnetization

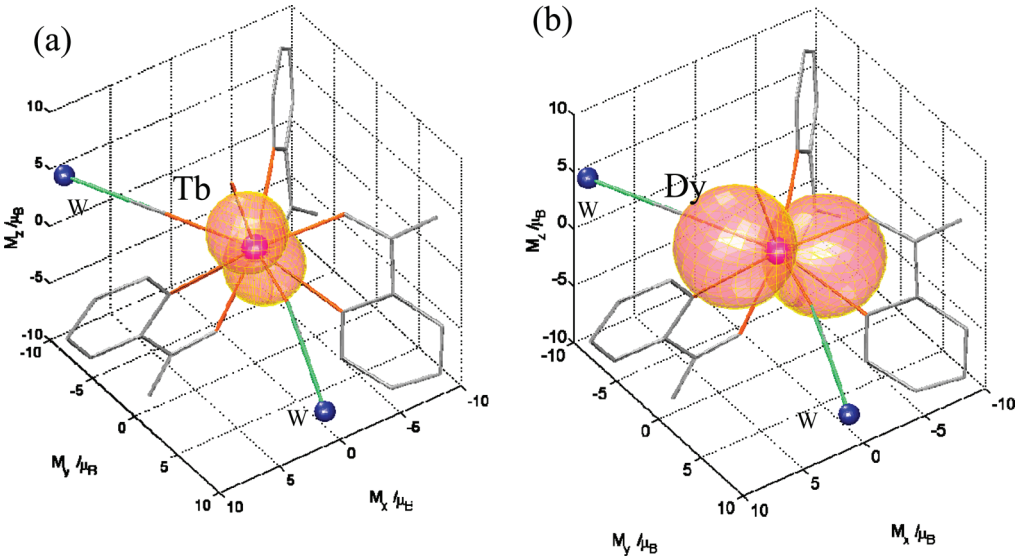

Figure 4. Computed magnetization surfaces (in Bohr magneton units, μ_B) for the ground levels of the (a) Tb(III) and (b) Dy(III) complex units. The molecular skeleton is figured in arbitrary units in order to visualize the orientation of the anisotropy with respect to the molecular frame. The orientation of the lobes represents the easy magnetization axis, their maximal extension being formally assignable to the $g_J \cdot J_z$ products, taken for maximal projections (J_z= ±6 and J_z= ±15/2 for Tb and Dy, respectively).

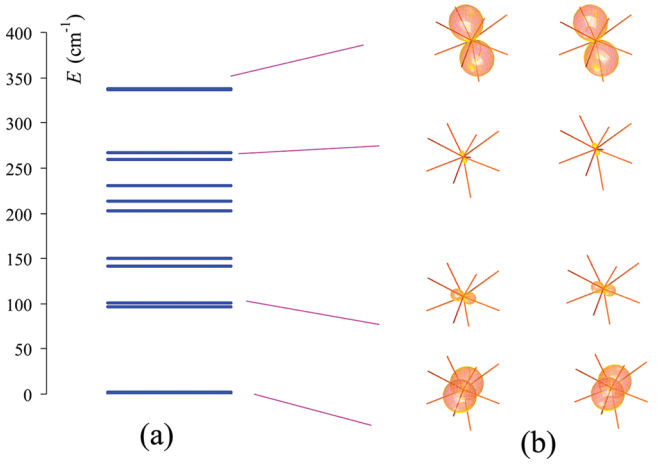

Figure 5. Magnetic anisotropy of the Tb(III) complex. (a) Computed lowest CASSCF-SO states, interpreted as the combined LF and SO effects in the split of a formal $^7F_6$ term. (b) Magnetization surfaces of the four lowest and four highest states of the spectrum. The intermediate levels show small extension of the magnetization lobes. Schematized molecular orientation is identical to those in Figure 4. The inset assigned here to the lowest state is the miniature of those in Figure 4a. All magnetization polar diagrams are represented obeying their relative magnitude.

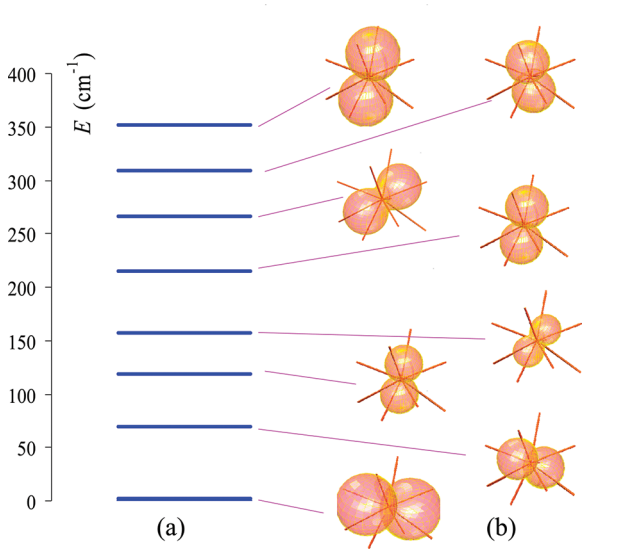

Figure 6. Magnetic anisotropy of the Dy(III) complex. (a) Computed lowest CASSCF-SO states, resulting from the combined LF and SO effects on the formal $^6H_{15/2}$ term. (b) Magnetization tensors for all states of the spectrum. Note that each level is doubly degenerate, the corresponding companions having identical magnetization tensors (depicted only once in the right side panel). The inset for the lowest state is the miniature of Figure 4b.

surfaces as small insets. The actual orientation of the molecular frame is the same as that in Figure 4, and the lowest component is equivalent to those depicted magnified in Figure 4a. Therefore, the insets in Figure 5b can be qualitatively compared each to other. The calculation revealed that while having a relatively high effective magnetic moment in the first two states, this drops rapidly, having smaller lobes for the magnetization tensors of states 3 and 4 (about 2.5 μB) and sensibly lower magnitudes for the next following states (between 0.5 and 1 μB). The magnitude rises again for the upper states, revealing a nonmonotonous pattern, i.e., mechanisms more complicated than those known for the regular ZFS effects. The fact that the lowest states of the LF-SO scheme are doubly degenerate for Dy(III) and quasi-doublet for Tb(III) validates the description of the system as a S = 1/2 pseudospin. The larger effective J_z moments are in fact absorbed in the g factors largely exceeding the ideal values, e.g., g_{Tb} = 5.6 parameter as described earlier.[22a]

For the Dy(III) compound (Figure 6) the situation is a bit different. In this case, all states carry a non-negligible magnetic moment. Visual comparison of the magnetization lobes in Figure 6b shows that the effective maximal moment is reached

dx.doi.org/10.1021/ic201427w |*Inorg. Chem.* 2011, 50, 9678–9687

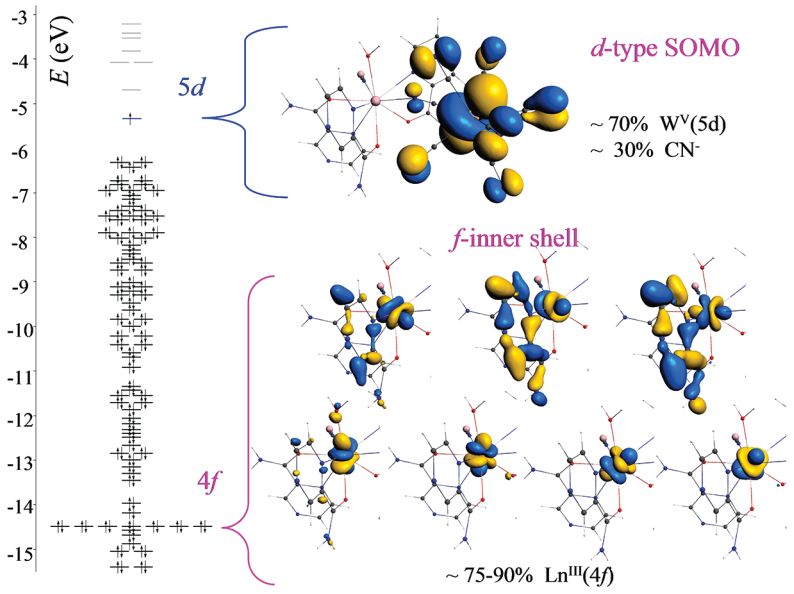

Figure 7. Orbitals of the $[Lu(pzam)_3(H_2O)(NCLi)][Wo(CN)_8]$ model dimer. Selected MOs, the SOMO with $5d^1$ character, and the f-type components are presented on the left site. They are detailed on the right side. Note that the orbitals having f nature are placed deep inside the energy scale, a fact that causes a non-aufbau pattern in the case of paramagnetic lanthanide complexes. The Lu(III) avoided the non-aufbau situation due to the closed f^{14} shell.

at the ground state. This is followed by a drop in effective magnetization for the next states and a new increase toward the end of the sequence. There is no simple relationship between the distribution of the effective magnetization among the states of the LF-SO spectra and the experimental recorded magnetization. At a first glance, we attempted to assign the nonmonotonous distribution of the effective $g_J J_z$ magnetization amounts from the computed spectrum as determining the pattern of the χT curve along the whole temperature range. However, ab initio simulation of the magnetic susceptibility probed that the lowest part of the experimental dependence cannot be assigned to the lanthanide ion, as initially attempted. In spite of the apparent reasons that may suggest a possible drop in χT of compounds **2** and **3** on the ground of effective decrease of the $g_J J_z$ amount along the lowest states, complete simulation shows that this is a false intuition. The simplified numerical experiments in the Supporting Information illustrate this fact and the importance of working with complete formalism of the magnetic susceptibility, instead of immediate approximations.

Calculation on the Gd(III) system reveals a ZFS pattern, well fitted with the following parameters: $D = 0.034$ cm^{-1} and $E = 0.005$ cm^{-1}. Although small, these parameters can be significant for the low-temperature magnetism. The ZFS on Gd(III) comes from weak interaction of the ground state spin octet (^8S) with the excited low-spin states, which for the pure ion are ^6P, ^6I, ^6D, ^6G, ^6F, and ^6H. The calculation included the correspondence of all states in the molecular unit, the output relevant for the ZFS effect being retrieved from the lowest 8 levels of the full CASSCF-SO spectrum. The computed ZFS is in line with those fitted, as discussed at the beginning of section 3.1.

The ab initio calculations presented herein are accounting for the magnetism and implicitly for LF effects, in a reasonable semiquantitative manner. This brings a fresh perspective in deciphering the complexity of lanthanide LF modeling. We will not aim here to decompose the actual ab initio results in the frame of a LF parametrization, since this is a separate technical insight, emphasizing in turn the possibility of direct shortcuts via the ab initio approach.

3.3. DFT Analysis of Coordination and Assembling Effects. In this section we will illustrate in a pictorial manner the issue of the non-aufbau structure of lanthanide complexes and expose considerations related to the molecular and supramolecular association. In order to use more accessible methods such as density functional theory, we used Lu(III) as a replacement for lanthanide ions, taking the molecular fragments from the experimental structures of the Tb(III)−W(V) chain. The filled f^{14} configuration of lutetium prevents the problems related with the non-aufbau configuration of paramagnetic lanthanide ions, enabling the DFT regular treatment.

For purposes regarding the overall bonding regime, ignoring magnetic issues, the diamagnetic Lu(III) ions can be reasonably used as a surrogate of actual lanthanides in the molecular models.[13] This is because the f shell is well confined inside the lanthanide ion and does not contribute to the bonding.[31] The corresponding numeric experiments for Lu(III) are illustrative for the whole series of lanthanides.[31] The impact of the so-called lanthanide contraction is minimal, Tb(III) and Lu(III) differing only about 3% in their averaged ionic radii.[25] Calculation of Lu(III) congeners affords, at one side, a reasonable tractability and, on the other side, illustrates the electron structure complications implied in the case of systems with partly filled f shells.

The non-aufbau issue on the lanthanide complexes can be visualized in Figure 7, showing the molecular orbitals from DFT calculation on the $[Lu(pzam)_3(H_2O)(NCLi)][W(CN)_8]$ fragment. One observes that the f shell is placed deep inside the energy scale, below many doubly occupied MOs pertaining to the ligands and to a neighboring coordination unit. The highest level is a singly occupied molecular orbital (SOMO) preponderantly (about 70%) consisting in a 5d atomic orbital from tungsten, i.e., in line with the d^1 configuration expected for the formal W(V) oxidation state. The SOMO has z^2 appearance, with the main lobes oriented toward the quasi-rectangular faces of an approximate

dx.doi.org/10.1021/ic201427w |*Inorg. Chem.* 2011, 50, 9678–9687

Table 1. Coordination Energies of All Ligands Inside the Presented d and f Fragments and for Their Association into the $[Lu(pzam)_3(H_2O)(NCLi)][W(CN)_8]$ Complex

	E (kcal/mol)		
	$[W(CN)_8]^{3-}$	$[Lu(pzam)_3(H_2O)(NCLi)]^{3+}$	{Lu−W} complex
Pauli repulsion	751.3	166.5	49.2
electrostatic interaction	−4143.0	−485.6	−461.2
orbital effects	−2188.4	−407.6	−93.8
total bonding energy	−5580.10	−726.7	−505.8

square antiprism. The doubly occupied HOMOs are mainly from the $[W(CN)_8]^{3-}$ fragment, while the empty LUMOs belong to the pzam ligand in the lanthanide coordination sphere, suggesting the possible importance of charge transfer effects.

While the SOMO is labeled as the 234th MO, the levels resembling the f lanthanide shell are encountered in the 154−161 sequence of the orbital count of the Lu−W dimer. Four MOs from this set show the expected f pure character, with f contents around 90%. The three others are accidentally mixed with components, having only 75−80% f content. Considering the $[Lu(pzam)_3(H_2O)(NCLi)]$ mononuclear unit alone, the f shell is also placed low in the energy scale, as MO nos. 89−96. However, in the mononuclear unit the MOs are closer to the AO status, having about 95−98% f content. The mixing between f AOs and the ligand components in the Lu−W model dimer is a rather artificial effect. This cannot be however avoided in the single-determinant methods, if distant or weakly interacting fragments happen to have accidentally degenerate energies.

In DFT, the non-aufbau configurations as well as numeric experiments with fractional spin and orbital populations are conceptually allowed.[32] These are well implemented in the ADF code.[33] However, even with these advanced capabilities in controlling MO occupations, it is practically impossible to work safely the complicated electron schemes of large lanthanide complexes. These have many MOs that accidentally interfere with the partly filled f shell. Our repeated attempts using various technical strategies led to severe convergence problems when using paramagnetic lanthanide ions in DFT calculations. In spite of the fact that there are few remarkable cases that succeeded the use of DFT for open-shell lanthanide systems,[34] the DFT approach to f complexes is not a full warranty routine method.[28] The nature of these difficulties illustrates in fact the physical features of the interactions implying the f shell. This is a weakly interacting subsystem, which cannot be treated properly in single-determinant methods, as is the case of DFT. Conversely, multideterminant methods as used in the previous section are more appropriate to treat the regime of weak interacting systems. This is because of the right account of static correlation, absolutely necessary in such circumstances.

We clearly illustrated that the f shell in complexes is far from frontier MO character and therefore escapes to common intuition and techniques related to the DFT practice. In a paramagnetic lanthanide ion, the f components will show a similar placement, deep down on the energy scale, facing then a structure with severe non-aufbau features. The pointing of such aspect is a part of the message intended in this section, focusing after this to estimation of the coordination and supramolecular association energies.

Table 2. Association Energies for Individual Ligands in the $[Lu(pzam)_3(H_2O)(NCLi)_2]^{3+}$ Unit[a]

	E (kcal/mol)		
	$pzam_{(av)}$	H_2O	$NC-Li_{(av)}$
Pauli repulsion	66.2	34.3	45.2
electrostatic interaction	−14.5	−0.5	12.7
orbital effects	−109.8	−54.7	−113.2
total bonding energy	−58.1	−20.9	−55.3

[a] The three slightly different pzam ligands and the two NC bridges are presented as their corresponding average.

The ADF fragment energy decomposition scheme allowed us to estimate the energies of selected association stages. We present also the dichotomized components of the total energy: Pauli repulsion, electrostatic energy, and the orbital part.[35] The Pauli repulsion is a term of pure quantum nature that appears between the closed-shell subsystems.[36] The orbital part is the component assignable to covalence effects.[37]

Considering the W(V) ion and the isolated CN^- ligands vs the computed $[W(CN)_8]^{3-}$ unit, we obtain the results rendered in the first column of Table 1. One may see that the coordination strength (measured by the total bonding energy) is large in this unit. Mulliken population analysis shows that the bonding of lanthanide is realized by the involvement of virtual orbitals of the lanthanide, finding an increment of about 0.1 electrons in the 6s and 6p shells and 0.8 electrons in the 5d AOs. This suggests that the bonding is made by donation from ligands toward these outer shells. The Mulliken charge of the Lu(III) in complex is +1.98, which represents an overestimation of the occurred charge transfer. The Mulliken populations are conventional and approximate measures of the electron distribution between atoms, being rather inadequate in the case of polar bonding (because it divides in equal shares the overlap contributions, irrespective of the differentiated electronegativity). A better population scheme in such circumstances is Hirshfeld analysis.[38] The Hirshfeld charge of the lanthanide in complex is +2.77, suggesting a more realistic ionic scheme, with about 0.2 charge fraction accommodated mostly in the 5d orbitals. Analysis of the $[W(CN)_8]^{3-}$ unit shows, at the Mulliken level, a massive donation from cyanide toward the 5d shell of tungsten, so that its formal charge is negative, about −0.44. The Hirshfeld charge is, again, more realistic, giving the +3.24 effective charge on the W center. The effective charge, lower than the nominal oxidation state (+5), suggests a certain degree of covalence in this unit. The $[Lu(pzam)_3(H_2O)(NCLi)]^{3+}$ unit (second column of Table 1) analyzed with respect to Lu(III) and constituting ligands, considered all together as a single fragment, shows a smaller association energy. This is in line with the idea of ionic bonding. Finally, taking the cation complex $Lu(pzam)_3(H_2O)(NCLi)]^{3+}$ and the anion $[W(CN)_8]^{3-}$ as fragments, one obtains the supramolecular assembling energy, which is revealed to be of electrostatic nature.

Table 2 presents the quantities related to the binding of individual ligands in the $[Lu(pzam)_3(H_2O)(NCLi)_2]^{3+}$ unit. Here, both W−CN bridges from the chain were replaced with the NC−Li prosthetic groups. This numeric experiment detects the action of cyanide toward the lanthanide, eliminating the electrostatic part that appears at the supramolecular contact of full f and d units (as shown in Table 1). The formation energies

dx.doi.org/10.1021/ic201427w |Inorg. Chem. 2011, 50, 9678–9687

are estimated taking as fragments a given ligand and the remainder of the complex. For instance, estimation of one pzam ligand implies the preliminary preparation of the pzam and $[Lu(pzam)_2(H_2O)(NCLi)_2]^{3+}$ fragments. Then the whole complex is assembled with respect to these components in the specific manner implemented in the ADF code. The quantities outlined in Table 2 belong to the output of such calculation. One observes the relatively high coordination strength of the cyanide moiety itself, comparable with those of the chelatic pzam groups. The two (NCLi) groups of this model structure show similar bonding energy components. Here, it is presented as their average. The three pzam ligands are similar each to other, the results being displayed on average. The aqua ligand appears with the lowest coordination power.

4. CONCLUSIONS

The magnetic properties of a new series of isostructural congeners displaying d−f chain topology were discussed from the viewpoint of both experimental and theoretical studies. State of the art computations afforded insight into the magneto-structural correlations of the discussed systems. The calculations consisted of nonroutine original methodologies employing CASSCF-SO procedures for description of combined effects of ligand field (LF) and spin−orbit (SO) coupling in determining the magnetic anisotropy of the considered lanthanide units. The ab initio obtaining of the magnetization polar diagrams for each state of the lowest multiplets as well as the first-principles simulation of susceptibility a good match with the experimental pattern represent original elements of the work presented herein. We studied the effects behind the association of molecular constituents in complex units and of the coordination fragments into the extended structure. The energy decomposition scheme available in the ADF code enabled us to compare the coordination strengths of the ligands in the d and f units and also to estimate supramolecular effects of the d−f assembling. The actual results and discussions draw the line of potential new developments and challenges in a new generation of magneto-structural studies on lanthanide compounds.

■ ASSOCIATED CONTENT

Supporting Information. Elemental analysis, IR, and XRD data for compounds **1**−**3** and description of the simulation performed on the magnetic susceptibility data. This material is available free of charge via the Internet at http://pubs.acs.org.

■ AUTHOR INFORMATION

Corresponding Author

*E-mail: s.grecea@uva.nl (S.T.); marilena.cimpoesu@g.unibuc.ro (M.F.).

■ ACKNOWLEDGMENT

This research was supported by a Veni grant from The Netherlands Organization for Scientific Research (NWO) to S.T. M.F. acknowledges funds from the research grant CNCSIS-UEFISCDI PN2-Idei 467/2009 and PN2-PCCE 9/2010.

■ REFERENCES

(1) Cotton, S. *Lanthanide and actinide chemistry*; John Wiley & Sons: New York, 2006.

(2) (a) Benelli, C.; Gatteschi, D. *Chem. Rev.* **2002**, *102*, 2369−2388 and references therein. (b) Sakamoto, M.; Manseki, K.; Okawa, H. *Coord. Chem. Rev.* **2001**, *219*−*221*, 379-414 and references therein.

(3) Christou, G.; Gatteschi, D.; Hendrickson, D. N.; Sessoli, R. *MRS Bull.* **2000**, *25*, 66–71.

(4) Gatteschi, D.; Sessoli, R. *Angew. Chem., Int. Ed.* **2003**, *42*, 268–297.

(5) (a) Zaleski, C. M.; Depperman, E. C.; Kampf, J. W.; Kirk, M. L.; Pecoraro, V. L. *Angew. Chem., Int. Ed.* **2004**, *43*, 3912–3914. (b) Mishra, A.; Wernsdorfer, W.; Abboud, K. A.; Christou, G. *J. Am. Chem. Soc.* **2004**, *126*, 15648–15649.

(6) Costes, J. −P.; Dahan, F.; Wernsdorfer, W. *Inorg. Chem.* **2006**, *45*, 5–7.

(7) (a) Ishikawa, N.; Sugita, M.; Wernsdorfer, W. *J. Am. Chem. Soc.* **2005**, *127*, 3650–3651. (b) Ishikawa, N.; Sugita, M.; Wernsdorfer, W. *Angew. Chem., Int. Ed.* **2005**, *44*, 2931–2935.

(8) Nockemann, P.; Thijs, B.; Postelmans, N.; Van Hecke, K.; van Meervelt, L.; Binnemans, K. *J. Am. Chem. Soc.* **2006**, *128*, 13658–13659.

(9) Koch, W.; Holthausen, M. C. *A Chemist's Guide to Density Functional Theory*; Wiley-VCH: Berlin, 2001.

(10) Paulovic, J.; Cimpoesu, F.; Ferbinteanu, M.; Hirao, K. *J. Am. Chem. Soc.* **2004**, *126*, 3321–3331.

(11) Ferbinteanu, M.; Kajiwara, T.; Choi, K.-Y.; Nojiri, H.; Nakamoto, A.; Kojima, N.; Cimpoesu, F.; Fujimura, Y.; Takaishi, S.; Yamashita, M. *J. Am. Chem. Soc.* **2006**, *128*, 9008–90009.

(12) Ferbinteanu, M.; Kajiwara, T.; Cimpoesu, F.; Katagiri, K.; Yamashita, M. *Polyhedron* **2007**, *26*, 2069–2073.

(13) Ferbinteanu, M.; Cimpoesu, F.; Kajiwara, T.; Yamashita, M. *Solid State Sci.* **2009**, *11*, 760–765.

(14) Kahn, M. L.; Mathoniere, C.; Kahn, O. *Inorg. Chem.* **1999**, *38*, 3692–3697.

(15) Tanase, S.; Reedijk, J. *Coord. Chem. Rev.* **2006**, *250*, 2501–2510.

(16) (a) Przychodzeń, P; Lewiński, K.; Pełka, R.; Bałanda, M.; Tomala, K.; Sieklucka, B. *Dalton Trans.* **2006**, 625. (b) Estrader, M.; Ribas, J.; Tangoulis, V.; Solans, X.; Font-Bardia, M.; Maestro, M.; Diaz, C. *Inorg. Chem.* **2006**, *45*, 8239. (c) Figuerola, A.; Ribas, M.; Casanova, D.; Maestro, M.; Alvarez, S.; Diaz, C. *Inorg. Chem.* **2005**, *44*, 6949. (d) Liu, S.; Plecnik, C. E.; Meyers, E. A.; Shore, S. G. *Inorg. Chem.* **2005**, *44*, 282. (e) C.; Ribas, J.; Tangoulis, V.; Sangregorio, C.; Gatteschi, D.; Maestro, M.; Mahia, J. *Inorg. Chem.* **2003**, *42*, 5274.

(17) Newman, D. J.; Ng, B. K. C. *Crystal Field Handbook*; Cambridge University Press: Cambridge, 2000. Edvardsson, S.; Åberg, D. *Comput. Phys. Commun.* **2001**, *133*, 396–406.

(18) Figgis, B.N.; Hitchman, M.A. *Ligand Field Theory and its Application*; Wiley−VCH: New York, 2000.

(19) Sorace, L.; Sangregorio, C.; Figuerola, A.; Benelli, C.; Gatteschi, D. *Chem.—Eur. J.* **2009**, *15* (6), 1377–1388.

(20) (a) Ishikawa, N.; Sugita, M.; Okubo, T.; Tanaka, N.; Iino, T.; Kaizu, Y. *Inorg. Chem.* **2003**, *42*, 2440–2446. (b) Ishikawa, N.; Iino, T.; Kaizu, Y. *J. Phys. Chem. A* **2002**, *106*, 9543–9550. (c) Ishikawa, N. *J. Phys. Chem. A.* **2003**, *107*, 5831–5835.

(21) Przychodzeń, P; Pełka, R.; Lewiński, K.; Supel, J.; Rams, M; Tomala, K.; Sieklucka, B. *Inorg. Chem.* **2007**, *46*, 8924–8938.

(22) (a) Prins, F.; Pasca, E.; de Jongh, L. J.; Kooijman, H.; Spek, A. L.; Tanase, S. *Angew. Chem., Int. Ed.* **2007**, *46*, 6081–6084. (b) Tanase, S.; Evangelisti, M.; de Jongh, L. J.; Smits, J. M. M.; de Gelder, R. *Inorg. Chim. Acta* **2008**, *361*, 3548–3554.

(23) (a) Tanase, S.; de Jongh, L. J.; Prins, F.; Evangelisti, M. *ChemPhysChem* **2008**, *9*, 1975–1978. (b) Tanase, S.; Evangelisti, E.; de Jongh, J. L. *Dalton Trans.* **2011**, *40*, 8407–8413.

(24) Schmidt, M. W.; Baldridge, K. K.; Boatz, J. A.; Elbert, S. T.; Gordon, M. S.; Jensen, J. H.; Koseki, S.; Matsunaga, N.; Nguyen, K. A.; Su, S. J.; Windus, T. L.; Dupuis, M.; Montgomery, J. A. *J. Comput. Chem.* **1993**, *14*, 1347–1363.

(25) (a) Stevens, W. J.; Basch, H.; Krauss, M. *J. Chem. Phys.* **1984**, *81*, 6026–6033. (b) Stevens, W. J.; Krauss, M.; Basch, H.; Jasien, P. G. *Can. J. Chem.* **1992**, *70*, 612–630. (c) Cundari, T. R.; Stevens, W. J. *J. Chem. Phys.* **1993**, *98*, 5555–5565.

(26) (a) ADF2006.01, SCM, Theoretical Chemistry, Vrije Universiteit, Amsterdam, The Netherlands, http://www.scm.com. (b) te Velde, G.; Bickelhaupt, F. M.; van Gisbergen, S. J. A.; Fonseca Guerra,

C.; Baerends, E. J.; Snijders, J. G.; Ziegler, T. *J. Comput. Chem.* **2001**, *22*, 931–967. (c) Fonseca Guerra, C.; Snijders, J. G.; te Velde, G.; Baerends, E. J. *Theor. Chem. Acc.* **1998**, *99*, 391–403.

(27) (a) Becke, A. D. *Phy. Rev. A* **1988**, *38*, 3098–3100. (b) Perdew, J. P. *Phys. Rev. B* **1986**, *33*, 8822–8824. (c) Perdew, J. P. *Phys. Rev. B* **1986**, *34*, 7406.

(28) Verdaguer, M.; Gleizes, A.; Renard, J. P.; Seiden, J. *Phys. Rev. B* **1984**, *29*, 5144–5155.

(29) (a) Nakano, H.; Nakayama, K.; Hirao, K.; Dupuis, M. *J. Chem. Phys.* **1997**, *106*, 4912–4917. (b) Roos, B. O.; Andersson, K.; Fulscher, M. K.; Malmqvist, P.-A.; Serrano-Andres, L.; Pierloot, K.; Merchan, M. *Adv. Chem. Phys.* **1996**, *93*, 219–331.

(30) (a) Pierloot, K. In *Computational Organometallic Chemistry*; Cundari, T., Ed.; Marcel Dekker, Inc.: New York, 2001; pp 123−158.

(31) Cotton, F. A.; Wilkinson, G. *Advanced Inorganic Chemistry*, 5th ed.; John Wiley: New York, 1988; pp 776, 955.

(32) (a) Gross, E. K. U.; Oliveria, L. N.; Kohn, W. *Phys. Rev. A* **1988**, *37*, 2809–2820. (b) Gross, E. K. U.; Oliveria, L. N.; Kohn, W. *Phys. Rev. A* **1988**, *37*, 2809–2820. (c) Ullrich, C. A.; Kohn, W. *Phys. Rev. Lett.* **2001**, *87*, 093001–093004. (d) Cances, E. *J. Chem. Phys.* **2001**, *114*, 10616–10621.

(33) te Velde, G.; Bickelhaupt, F. M.; Baerends, E. J.; Fonseca Guerra, C.; Van Gisbergen, S. J. A.; Snijders, J. G.; Ziegler, T. *J. Comput. Chem.* **2001**, *22*, 931–967.

(34) (a) Zbiri, M.; Atanasov, M.; Daul, C.; Garcia-Lastra, J. M.; Wesolowski, T. A. *Chem. Phys. Lett.* **2004**, *397*, 441. (b) Borel, A.; Helm, L.; Daul, C. A. E. *Chem. Phys. Lett.* **2004**, *383*, 584–591. (c) Rajaraman, G.; Totti, F.; Bencini, A.; Caneschi, A.; Sessoli, R.; Gatteschi, D. *Dalton Trans.* **2009**, 3153–3161.

(35) Dykstra, C. E.; Frenking, G.; Kim, K. S.; Scuseria, G. E. *Theory and Applications of Computational Chemistry*; Elsevier B. V.: Amsterdam, 2005; p 291.

(36) Gritsenko, O. V.; Schipper, P. R. T.; Baerends, E. J. *Phys. Rev. A* **1998**, *57*, 3450–3457.

(37) Ferbinteanu, M.; Zaharia, A.; Gîrţu, M. A.; Cimpoesu, F. *Cent. Eur. J. Chem.* **2010**, *8*, 519–529.

(38) Hirshfeld, F. L. *Theor. Chim. Acta* **1977**, *44*, 129.